Particle-in-cell simulation study about the spatial distribution of DC magnetron sputtering plasmas with various magnetic field configurations

Y. H. Jo[1] , G. Park[1] and S. K. Nam[1]

[1] *Mechatronics Research, Samsung Electronics, Hwaseong, South Korea*

Abstract: The effects of various magnetic field configurations on the spatial distribution of DC magnetron sputterig (DCMS) plasmas have been investigated using two dimensional particle-in-cell Monte Carlo collisions (PIC-MCC) simulations. The influences of different locations of permanent magnets on the sputtering target and the effects of relatively weak magnetic fields from additional magnets placed around the chamber in the DCMS system are discussed in this study.

Keywords: PIC-MCC simulation, DC magnetron sputtering, spatial distribution.

1. Introduction

Magnetron sputtering (MS) is one of the physical vapor deposition (PVD) technologies for thin-film coatings. The MS system generates high-density plasmas to sputter target materials at the pressures lower than a few mTorr. A conceptual layout of the typical MS system is depicted in Fig. 1. Target atoms sputtered by ions of plasmas fall into and deposited on the substrate at the anode side. The permanent magnets in the MS system, which typically consist of inner and outer magnets where magnetic poles of them are opposite to each other, confine plasmas near the sputtering taret. The magnetic field intensity below the sputtering target area is typically in the range from hundreds of Gauss to a few thousands of Gauss. In this condition, most of the electrons in this system are trapped in the region where magnetic fields are parallel to the sputtering target. Those trapped electrons rotate in the azimuthal direction with cycloid-like motions due to crossed electric and magnetic fields, while ions in this stem are barely confined since the gyro-radius of a heavy ion is either similar as the system length or bigger than the system length. In other words, electrons are strongly magnetized while ions are weakly magnetized in the MS system.

DC magnetron sputtering (DCMS) can be utilized for metal coatings. It is not possible to sustain plasmas with dielectric targets in the DCMS system due to accumulation of positive charges on the targets. AC magnetron sputtering or high-power impulse magnetron sputtering (HiPIMS) can be utilized for dielectric coatings instead. This research aims to investigate physics of the DCMS plasma and its spatial distribution in various magnetic configurations. The spatial distribution of plasmas in the MS system highly depends on the behaviors of the magnetized electrons. Therefore, electron kinetics should be treated very accurately to investigate the plasma discharges in the MS system using simulations.

Particle-in-cell Monte Carlo collisions (PIC-MCC) simulation has been regarded as the most accurate method to simulate plasma discharges, especially the low-pressure plasmas in the MS system. The electromagnetic fields are calculated by solving the Maxwell equation, and the forces applied to the charged particles from the electromagnetic fields are calculated by solving the Newton-Lorentz equation. Both of the equations are solved iteratively with an appropriate time step which should be small enough to suppress the numerical errors. If an electrostatic system is considered, the field information is computed by solving the Poisson equation instead of the Maxwell equation. MCC is a computational method to simulate the collisions of particles efficiently with a preprocess that selects particles to be collided, which is widely used to date [1].

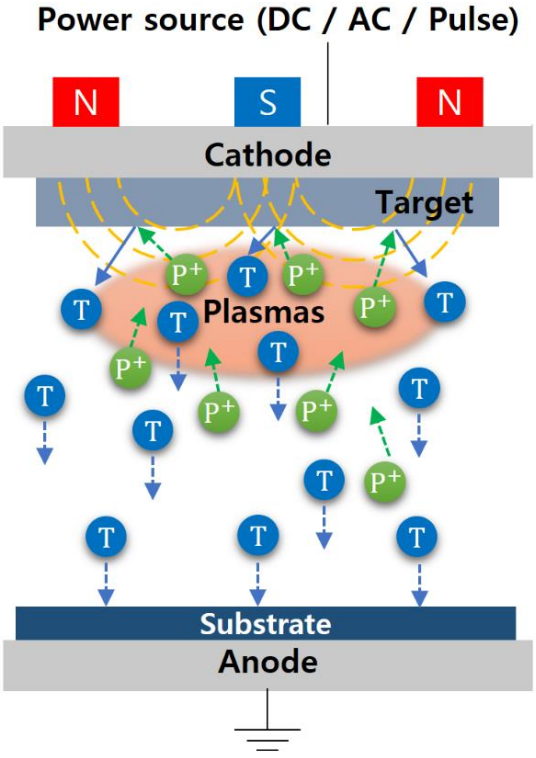

Fig. 1. A conceptual layout of the MS system.

The effects of various magnetic field configurations on MS plamsas are investigated in the previous researches with both experiments and simulations [2-12]. This study focuses on the influence of the radial position of permanent magents on the target plate and an additional electromagnet on the spatial distribution of plasmas in the DCMS system.

2. Computational details

A newly developed two dimensional electrostatic PIC-MCC code is utilized in this study. The code is developed

in the Cartesian coordinates to avoid numerical problems caused by different cell sizes depending on the radial position in the cylindrical coordinates. In this code, the conventional finite different method (FDM) and the preconditioned conjugate gradient (PCG) algorithm are applied to solve the Poisson equation. The Boris method and the leap-frog scheme are applied to solve the Newton-Lorentz equation. This code is parallelized using CUDA, and performed by a high-performance GPU. The computing speed of this code is more than 100 times faster than the speed of a conventional PIC-MCC code performed using a single CPU.

A schematic diagram of the simulation domain and the profile of magnetic fields are shown in Fig. 2. A DCMS system with an additional electromagnet is considered in this study. It has one cathode at the top with permanent magnets which confine most of the plasmas in this system. A Cu plate is the sputtering target, which is also considered as a cathode in this study. The power applied to the cathode is 100W. The other conductors of the chamber are all grounded. They are placed below the target plate where a very thin Al_2O_3 ring which has a releative permittivity of 9.8 is placed between the target plate and the grounded conductors. The magnetic fields are calculated using Ansys Maxwell and applied to the simulation as external static fields. The number of turns in the coil of the electromagnet is 100. The current applied to the electromagnet is 20 A. Plasma simulations are performed inside the chamber.

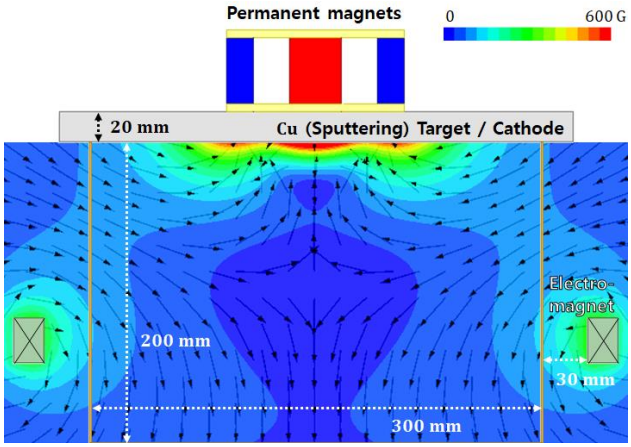

Fig. 2. A schematic diagram of the simulation domain and the profile of magnetic fields.

Table 1. Reactions of Ar considered in the model.

Reaction	Name	Reference
$e^- + Ar \rightarrow e^- + Ar$	Eleastic scattering	[13]
$e^- + Ar \rightarrow e^- + Ar^*$	Excitation	[13]
$e^- + Ar \rightarrow e^- + Ar^+$	Direct ionization	[13]
$Ar^+ + Ar \rightarrow Ar^+ + Ar$	Elastic scattering	[14]
$Ar^+ + Ar \rightarrow Ar + Ar^+$	Charge exchange	[14]

A pure Ar gas is considered as a feed gas in this study. Reactions of Ar applied in the simulation are listed in Table 1. The flow of the argon gas is not computed as we assume the gas is uniform inside the chamber. The ion-induced secondary electron emission coefficient (SEEC) of the Cu plate is set to be 0.2 for the sake of simplicity. The transition of the plasma discharges with sputtered target materials after ignition of plasmas is not considered in this study.

3. Preliminary results

Eletrostatic PIC-MCC simulation results of DCMS plasmas to invesitgate the influence of various magnetic field configurations on the spatial distribution of plasmas are shown in this section.

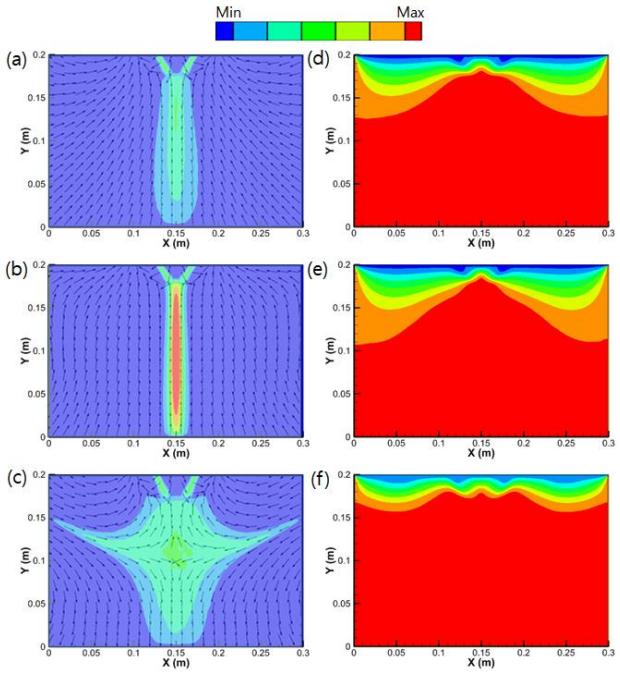

Fig. 3. Profiles of plasmas with permanent magnets on the center of the target plate: (Left) densities of electrons and magnetic fields with (a) no electromagnet, (b) an electromagnet with counter-clockwise currents, (c) an electromagnet with clockwise currents. (Right) electric potentials with (d) no electromagnet, (e) an electromagnet with counter-clockwise currents, (f) an electromagnet with clockwise currents.

Fig. 3 depicts the spatial profiles of plasmas with different conditions of the electromagnet where permanent magnets are placed on the center of the target plate. The voltage applied to the cathode is -300 V when there is no electromagnet. The permanent magnet of this study confines plasmas not only near the target but in the middle region with a tail-like shape which touches the substrate without any additional electromagnet as shown in Fig. 3(a). Fig. 3(b) represents that the magnetic fields of the electromagnet with counter-clockwise currents increase the plasma density in the tail-like region by more than 100% even though the magnetic field strength of the electromagnet applied to this region is less than 100 Gauss which is relatively lower than the one of the permanent

mangets. The electric potentials shown in Fig. 3(d) and Fig. 3(e) seem similar with the same voltage at the cathode. On the other hand, Fig. 3(c) shows that the electromagnet with clockwise currents does not increase the plasma density much but changes the spatial distribution of plasmas significantly. It is caused by a magnetic null point at the center of the domain. It also makes the wing-like distribution of plasmas, which extends the region of plasmas inside the chamber. The voltage applied to the cathode is about -250 V as shown in Fig. 3(f), which means that more easily confined plasmas could be sustained by relatively lower discharge voltages in this case.

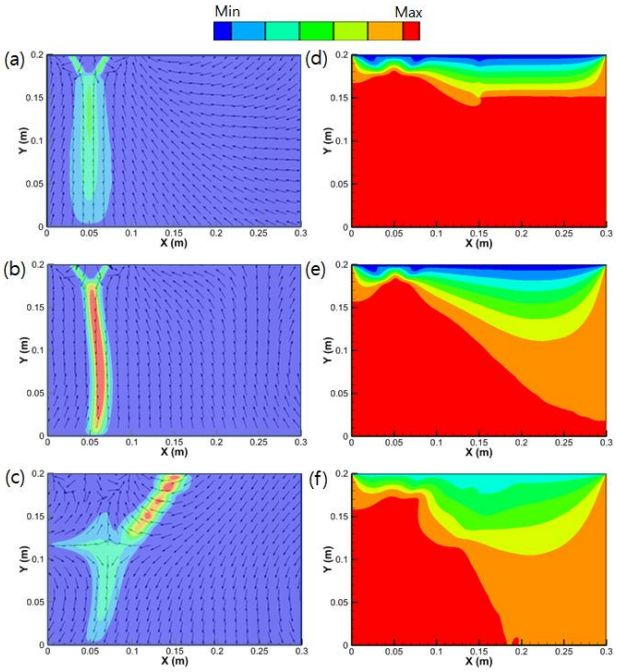

Fig. 4. Profiles of plasmas with permanent magnets on the edge of the target plate: (Left) densities of electrons and magnetic fields with (a) no electromagnet, (b) an electromagnet with counter-clockwise currents, (c) an electromagnet with clockwise currents. (Right) electric potentials with (d) no electromagnet, (e) an electromagnet with counter-clockwise currents, (f) an electromagnet with clockwise currents.

The same variations of the electromagnet shown in Fig. 3 are applied to the case with permanent magnets on the edge of the target, where the results are depicted in Fig. 4. The voltage applied to the cathode is -300 V when there is no electromagnet, which is the same as the one shown in Fig. 3. Fig. 4(a) represents that there is no siginificant changes when the permanent magnet is placed on the edge of the target except that the plasma density is decreased by about 5% due to the wall loss at the edge region. Fig. 4(b) shows similar effects of the electromagnet with counter-clockwise currents on the plasmas as discussed with Fig. 3(b). However, the result becomes very different when the electromagnet with clockwise currents are applied. The region of plasmas near the target is not the same as the one in other conditions. Magnetic fields made by the magnetic null point confine plasmas more than the magnetic fields of the permanent magnet confine. The cathode voltage is about -200V in this case as shown in Fig. 4(f), which is significantly lower than the cathode voltages shown in Fig. 4(d) and Fig. 4(e). It represents that relatively low magnetic fields of electromagnets confine plasmas more easily, which is not so intuitive. The coupled effect of both asymmetry of magnetic fields and the magnetic null point could be the source of this result, but the fundamental reason is not fully investigated yet.

All of these changes are driven by the additional magnetic fields of which the strength is less than 100 Gauss. These results refers to the controllability of the plasma distribution with additional magnets in a DCMS system.

4. Discussions

The effects of various magnetic field configurations on the spatial distribution of DCMS plasmas are investigated with two dimensional electrostatic PIC-MCC simulations in this study. The additional magnetic fields from the electromagnet modify the spatial distributions of DCMS plasmas in various ways. They affect not only the region near the target plate but also the middle and bottom region of the chamber. The relatively low magnetic fields of the electromagnet make significant changes, especially when the permanent magnets are placed on the edge of the target plate. The detailed mechanism is not fully elaborated in this study, which will be investigated in future work.

5. References

[1] V. Vahedi and M. Surendra, Comput. Phys. Commun. **87**, 179 (1995).
[2] P. J. Kelly and R. D. Arnell, Vacuum **56**, 159 (2000).
[3] J. T. Gudmundsson, Plasma Sources Sci. Technol. **29**, 113001 (2020).
[4] G. Shanker, P. Prathap, K. M. K. Srivatsa, and P. Singh, Curr. Appl. Phys. **19**, 697 (2019).
[5] J. Alami, V. Stranak, A. P. Herrendorf, Z. Hubicka, and R. Hippler, Plasma Sources Sci. Technol. **24**, 045016 (2015).
[6] A. A. Solov'ev, N. S. Sochugov, K. V. Oskomov, and S. V. Rabotkin, Plasma Phys. Rep. **35**, 399 (2009).
[7] H. Yu, L. Meng, M. M. Szott, J. T. McLain, T. S. Cho, and D. N. Ruzic, Plasma Sources Sci. Technol. **22**, 045012 (2013).
[8] P. Raman, J. Weberski, M. Cheng, I. Shchelkanov, and D. N. Ruzic, J. Appl. Phys. **120**, 163301 (2016).
[9] G. Zhou, L. Wang, X. Wang, and Y. Yu, Surf. Coat. Technol. 409, 126837 (2021).
[10] S. Kim and K. H. Kim, Coatings **10**, 321 (2020).
[11] A. Kolesnikov, Y. Kryukov, M. Gafurov, and V. Bodnarchuk, Coatings **12**, 1807 (2022).
[12] F. Boydens, S. Mahieu, J. Haemers, and D. Depla, Phys. Status Solidi A **207**, 124 (2010).
[13] C. Yamabe, S. J. Buckman, and A. V. Phelps, Phys. Rev. A **27**, 1345 (1983).
[14] W. H. Cramer, J. Chem. Phys. **30**, 641 (1959).